

See discussions, stats, and author profiles for this publication at: <https://www.researchgate.net/publication/380509127>

A novel acceleration approach to shadow calculation based on sunlight channel for urban building energy modeling

Article in Energy and Buildings · May 2024

DOI: 10.1016/j.enbuild.2024.114244

CITATIONS

0

READS

6

5 authors, including:



Zhaoru Liu

Tsinghua University

11 PUBLICATIONS 127 CITATIONS

[SEE PROFILE](#)



Da Yan

Tsinghua University

273 PUBLICATIONS 10,264 CITATIONS

[SEE PROFILE](#)

1 A novel acceleration approach to shadow calculation based on sunlight channel
2 for urban building energy modeling

3 Zhaoru Liu^a, Xin Zhou^b, Xiaohan Shen^b, Hongsan Sun^a, Da Yan^{a,*}

4 ^a*Building Energy Research Center, School of Architecture, Tsinghua University, Beijing 100084, China*

5 ^b*School of Architecture, Southeast University, Nanjing 210096, Jiangsu, China*

6 **Abstract**

7 Shadow effect among buildings has great impacts on the building energy consumption and the performance of
8 building photovoltaic, and calculating shadows on building surfaces in urban building energy modeling (UBEM)
9 faces challenges of inefficiency, especially for dense urban areas. In this study, a novel shadow calculation approach
10 based on sunlight channel is proposed that can streamline the surrounding environment and accelerate the shadow
11 calculation process. The sunlight-channel algorithm can further accelerate the shadow calculation process by dy-
12 namically predetermining the shading surfaces according to the actual solar position. In a real urban context, the
13 proposed approach can accelerate the computation process by over 10 times over the baseline and over 34 times over
14 the non-accelerated method, with a mean absolute percentage error (MAPE) of 1.13% for the total solar radiation.
15 The proposed approach copes well with both large-scale urban models and the complexity of building structures,
16 particularly for urban models with complex changes in building heights. This approach can significantly enhance
17 the computational efficiency in complex urban environments, facilitating an accurate and rapid analysis of the energy
18 consumption and solar potential of buildings in dense cities.

19 *Keywords:* Shadow calculation, Urban environment, Polygon clipping, Building performance simulation, Urban
20 building energy modeling

21 **1. Introduction**

22 Cities are responsible for two-thirds of energy consumption and 70% of carbon emissions worldwide [1], and the
23 building sector constitutes approximately one-third of global carbon emissions and 30% of global energy consump-
24 tion. Therefore, buildings play an important role in achieving a sustainable, carbon-neutral future. Building energy
25 modeling (BEM) is an important technique for assessing building energy performance and has been widely used in
26 building design and operation [2].

*Corresponding authors

Email address: yanda@tsinghua.edu.cn (Da Yan)

27 *1.1. Significance and challenges in shadow calculation in the urban context*

28 Inter-building effects have been proven to have a significant impact on building energy performance and solar
29 energy use [3], particularly when the analysis is extended to a district or urban scale [4, 5]. Occlusion by surrounding
30 buildings is an important interbuilding effect [6] that affects the solar radiation received by building surfaces or sunlight
31 through glazing. Shading effects from nearby buildings can affect energy performance in many ways. [7] found that
32 the shading effects will lead to a decrease in cooling demand and an increase in heating demand, which depends on
33 different weather conditions and urban morphology. Shading effects also influence the indoor lighting environment
34 [8], and it is necessary to consider real urban environments. In addition, with the increasing penetration of building
35 PV systems, shading effects significantly impact PV installations [9, 10] and operational performance [11].

36 In addition, with the growing concern regarding energy consumption in urban buildings, urban building energy
37 modeling (UBEM) has been regarded as a potential toolkit to support the energy efficiency and sustainability of cities
38 [12, 13]. The approaches of UBEM are classified into two categories: top-down and bottom-up [14]. The bottom-up
39 physics-based approach generates BEMs automatically and simulates the energy performance of buildings [15, 16].
40 In bottom-up UBEM, shadow calculation is crucial, as it can reflect the heterogeneity in the dynamics of buildings
41 and neighborhoods [17].

42 Despite the significant impact of shading on building energy consumption and the indoor environment [18], it
43 is challenging to accurately and efficiently calculate shadows on building surfaces in a dense urban context [19].
44 On the one hand, with increasing building height and density due to rapid urbanization, more surrounding buildings
45 must be considered in shadow calculations. However, building structures are becoming increasingly complex. The
46 compactness and complexity of urban buildings have created challenges in shadow calculation because the shadows on
47 numerous building surfaces must be calculated based on all surrounding surfaces. The calculation time is proportional
48 to the square of the number of shaded surfaces [20], which limits the expansion of shadow calculations to larger
49 scales and more complex structures.

50 *1.2. Current shadow calculation methods*

51 Shadow calculations have been studied and applied in analyses of building energy performance and solar energy
52 use for over 30 years [21, 22]. There are three main approaches to calculating mutual beam shadows: ray tracing,
53 pixel counting, and polygon clipping [23, 24].

54 The ray-tracing approach simulates individual sunlight beams falling on surfaces bouncing around the scene [25].
55 This approach has been widely used in rendering algorithms in computer graphics because of its capability to simulate
56 scattering, reflection, and beam shadows. However, the surfaces must be divided into cells, and it is necessary to

57 determine the shadows cell-by-cell to calculate the shadowed areas on the surfaces [26, 27]. The finer the divided
58 surfaces, the more accurate the shading areas obtained; however, this is computationally intensive.

59 Pixel counting is based on GPU rendering for a fast approximation of the shaded area ratio [28]. In their method,
60 two image buffers were used to render the entire building: one including obstructions and the other without obstruc-
61 tions. Both the images were rendered using orthogonal projections from the vantage point of the sun. The number
62 of pixels belonging to each surface in both images was calculated and the fraction of each surface visible to the sun
63 was calculated by division [29]. This approach can handle complex geometries and achieves high computational ef-
64 ficiency based on graphics hardware [24]. However, the sampling resolution is limited in rendering for large-scale
65 environments because it is also a raster-based method; the geometric details may be neglected, and the shadow edges
66 may be distorted [30, 31]. In addition, the method has neither been integrated with building performance simulation
67 (BPS) software nor has it been widely implemented in urban-scale analysis.

68 Analytical approaches are based on projection transformations and polygon clipping [32]. The model was geomet-
69 rically transformed such that the surfaces that cast shadows were projected onto the receiving plane in the direction
70 of the suns rays. Subsequently, the remaining sunlit area is calculated by extracting the projected shadow polygons
71 from the receiving polygons using a process called polygon clipping [33]. This process was repeated for the exterior
72 surfaces of each building. Compared to cell-based approaches, polygon projection approaches are more accurate in
73 calculating the shape of the beam shadows. Currently, polygon clipping is widely used in most BPS software such as
74 EnergyPlus, DeST, ESP-r, and DOE-2. etc.

75 1.3. Acceleration approaches in shadow calculation

76 Despite their accuracy and wide applicability, analytical approaches face challenges in urban-scale building shad-
77 ow analysis. Although [34] found that polygon clipping was the most efficient approach compared with ray tracing
78 and pixel counting in urban scenes for surfaces with freely defined positions and orientations, the urban scene con-
79 tained only a small number of buildings. When simulating the entire urban building stock, which is equivalent to
80 millions of such urban scenes, it is necessary to make the model calculable and reduce the computation time of the an-
81 alytical method [35]. Many approaches have been applied to make the model calculable and accelerate the calculation
82 process based on the polygon-clipping approach. The first approach is to simplify the model, including the building
83 geometry or the number of shading surfaces [36]. Building models with fewer surfaces require less calculation time,
84 for example, combining the facades of multiple stories into one. [37] discussed the impact of the discretization of
85 facades on the efficiency and accuracy of the calculation of shading factors, and found that the model with detailed
86 floor configuration could be replaced by another parsimonious model of sufficient accuracy and higher simulation
87 speed.

88 In addition, the simplification of the surrounding environment setup is also an acceleration approach, which is
89 usually achieved by filtering the surrounding buildings based on distance. A distance threshold was used to identify
90 the shading surfaces [38], which is the distance between the target building and surrounding buildings. The larger the
91 distance threshold, the more accurate the shading factor, and the computation time increases accordingly. To balance
92 accuracy and efficiency, some studies proposed a criterion for the distance threshold as the height of the surrounding
93 building multiplied by the height multiplier [20]. The height multiplier was determined based on the local solar
94 altitude, which covers over 80% of the solar working time [17, 39]. [40] proposed the criterion for selecting the
95 minimum sun elevation angle based on the effective time belt (ETB).

96 Another approach is to accelerate the calculations. In contrast to filtering the surrounding buildings by distance in
97 the preprocess, the calculation process could also be improved at each time step or vantage point of the sun. Actually,
98 there are not many surfaces that may cast shadows on the target surface. Therefore, by filtering surfaces that are
99 unlikely to cast shadows on a target surface, the transformation, projection, and clipping of irrelevant surfaces can
100 be eliminated [41]. The number of surfaces can be reduced by screening for those that have no shading effect in
101 the current direction of light. [41] proposed an improved method for direct solar shading calculations. At each time
102 step, the surfaces were projected onto a unique plane orthogonal to the sunray instead of onto each of the potential
103 receiving surfaces. In addition, nonoverlapping, completely behind, and partially behind surfaces were eliminated
104 to avoid being processed in the polygon clipping. [42] proposed a neighborhood judgment approach to reduce the
105 neighborhood buildings at each solar azimuth, screening out the surrounding buildings in the solar azimuth quadrant.

106 Based on the above analysis, it was shown that the surrounding environment setup and the shadow calculation
107 process are two important aspects of acceleration. However, most current studies focus on the surrounding envi-
108 ronment setup to improve computational efficiency, while neglecting the potential of acceleration in the calculation
109 process. Although the quadrant filter approach by [42] can reduce the number of surfaces in the calculation process,
110 all the surfaces in the solar azimuth quadrant are calculated, some of which may also have no shading effect on the
111 target building. Because the surrounding environment setup and shadow calculation process are two sequential phases
112 in the analytical method, the acceleration techniques in each phase have the potential to synergize to achieve better
113 performance.

114 1.4. Aim and objectives

115 In light of the above analysis, this study proposes a sunlight channel technique to dynamically predetermine the
116 shading surface according to the actual solar position to further accelerate the shadow calculation process. An inte-
117 grated approach was proposed for shadow calculation on urban building surfaces by combining the existing distance

118 filtering method and sunlight channel technique, and the advantages and applicability of the proposed approach were
119 analyzed. This study contributes to existing literature in two ways.

- 120 • Proposal of a novel approach to shadow calculation based on sunlight channel for urban building energy mod-
121 eling, which could both accelerate the surrounding environment setup and the shadow calculation process.
122 • Assessment of the advantages and applicability of the proposed approach, and the impact of spatial scale and
123 height variation on the method performance, in terms of accuracy and computation time.

124 The remainder of this paper is organized as follows. Section 2 illustrates the proposed integrated approach, de-
125 scribes the case study, and presents a method of comparison. Section 3 compares the computational efficiency and
126 simulation results of different methods on parametric district building models and demonstrates the performance of the
127 proposed integrated approach in modeling a real urban environment. Section 4 presents the discussion, and Section 5
128 summarizes the contributions and significance of this study.

129 **2. Methodology**

130 The technical approach used in this study is illustrated in Fig. 1. The proposed method integrates distance filtering
131 and sunlight channels to improve the overall performance of the analytical method in UBEM. The proposed method
132 was compared with a state-of-the-art distance filtering method (baseline) and a non-accelerated method (ground truth).
133 Hypothetical shoebox buildings in a scalable neighborhood were selected as a case study, and the impacts of spatial
134 scale and height variation on accuracy and computation time were analyzed. The proposed method was applied to
135 real buildings in a central business district to evaluate their performances in real urban environments. All approaches
136 are based on an analytical method for shadow calculation, as introduced in Section 2.1.1. Workflow for the different
137 approaches are shown in Fig. 1.

138 *2.1. The proposed method*

139 The proposed method combines the distance filtering method and sunlight channel algorithm, which achieves both
140 simplification of the surrounding environment and acceleration of the calculation process, as shown in Fig. 1. When
141 calculating the shadows on a target building, the surrounding buildings with shading effects were screened using a
142 distance-filtering method to establish the shading scene. Subsequently, during the calculation process, buildings and
143 surfaces were further screened dynamically by establishing sunlight channels based on the position of the sun. Details
144 of the proposed method are provided below.

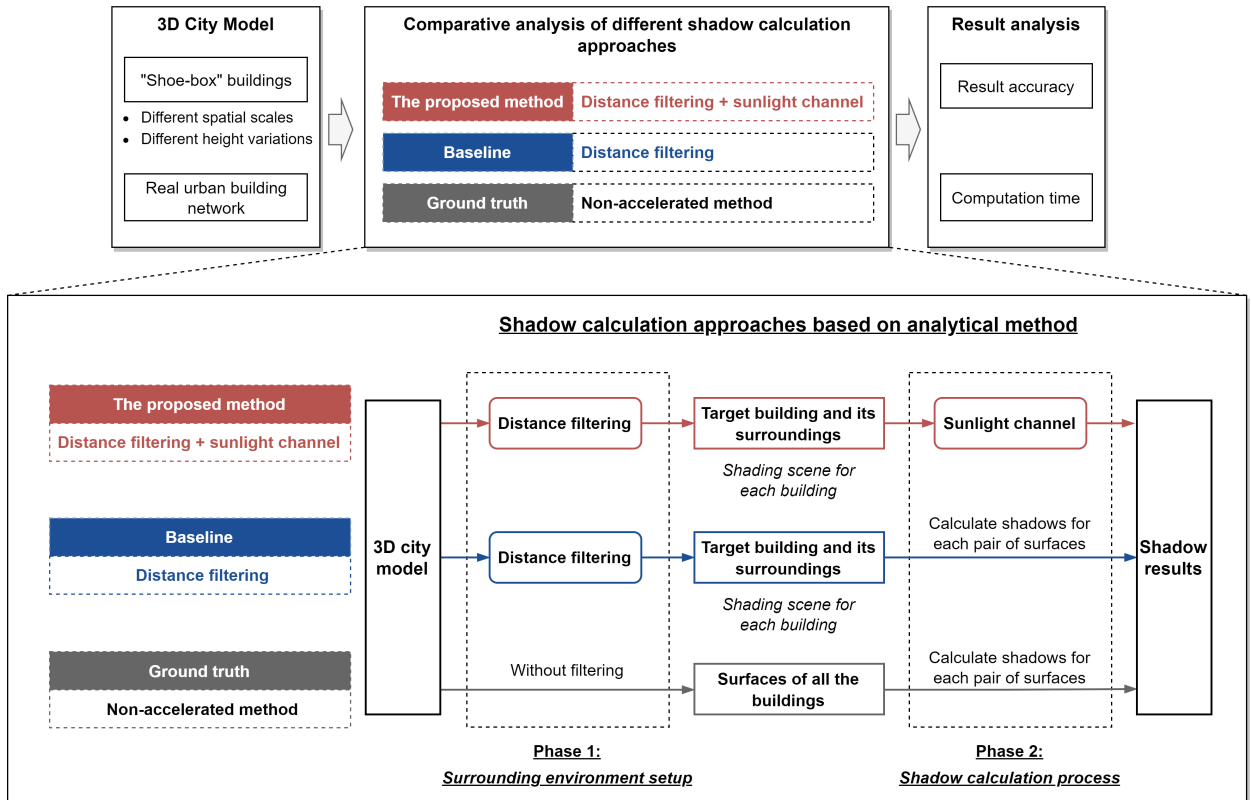


Figure 1: Technical approach of this study.

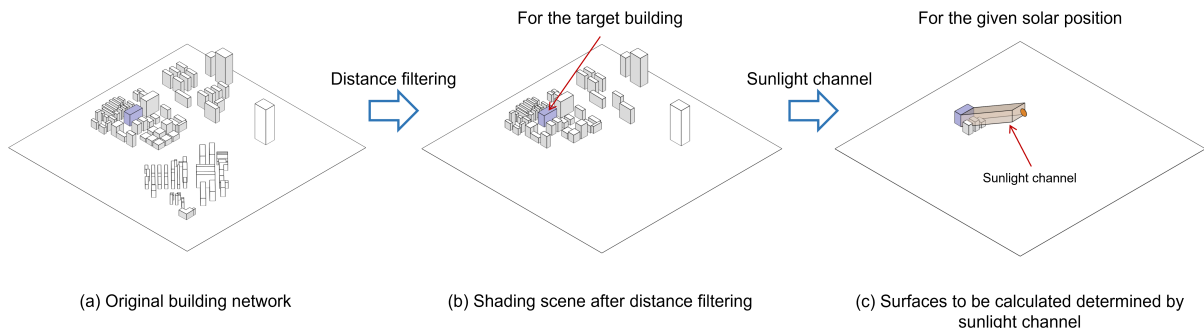


Figure 2: Decomposition process of the proposed method: (a) original building network, (b) shading scene after distance filtering, and (c) surfaces to be calculated determined by sunlight channel.

145 2.1.1. The analytical approach in shadow calculation

146 The analytical approach is based on projection transformation and polygon clipping, and was chosen as the main
 147 approach for shadow calculation in this study because of its wide applications in the shadow analysis of buildings.
 148 Shadow calculation is based on some basic assumptions: the sun is regarded as an ideal point light source, and the
 149 distance between the sun and the earth is much larger than the diameter of the earth. Therefore, the rays of light

150 can be regarded as parallel rays. In addition, only the umbra area of the beam shadow, which had absolute light and
151 dark boundaries, was calculated. In the typical workflow of an analytical approach, the shadow on a target surface is
152 calculated using the following steps [43]:

153 (1) Coordinate transformation: Take the surface to be calculated as the plain of projection, and transform the
154 surface to be calculated into the xoy plain coordinate system by the coordinate transformation matrix.

155 (2) Shadow projection: The same coordinate transformation is performed on the sunlight vector and other surfaces,
156 including both the surfaces of the surrounding buildings and other surfaces from the target building.

157 (3) Polygon clipping: Merge the projections of all surfaces on the xoy plane and then solve the intersection of the
158 merged shadow and the surface to be calculated, which is the shadow of the surface to be calculated.

159 (4) Inverse transformation: Inversely transform the obtained shadow calculation result on the xoy plane back to
160 the original coordinate system and obtain the shadow polygon on the surface to be calculated in real coordinates.

161 In existing approaches, the above steps must be performed for each building surface to be calculated. In addition,
162 each surface needs to follow the above steps with all the other surfaces individually to complete the shadow calculation
163 for the entire scene. Therefore, the shading algorithm is $O(n^2)$ when applied to all the surfaces.

164 2.1.2. *Distance filtering*

165 In distance filtering, the buildings in the neighborhood are filtered based on their distance to the target building in
166 the surrounding environment setup before the shadow calculation. In this study, the distance between the surround-
167 ing building and target building was compared with the height of the surrounding building multiplied by the height
168 multiplier to determine whether the surrounding building has a shading effect [20, 17]. The height multiplier was
169 determined as the cotangent value of the minimum solar altitude angle considered, which was 5.67 ($\approx \cot 10^\circ$) [39].
170 After filtering, only the remaining buildings are likely to cast shadows on the target buildings when the solar altitude
171 angle exceeds 10° , as shown in Fig. 2. This method is widely used in existing UBEM practices and represents the
172 current state of the art.

173 2.1.3. *Sunlight channel*

174 This study proposed the "sunlight channel" technique to further enhance the efficiency in the shadow calculation
175 at a given solar position. This concept is derived from collision detection in computer graphics, which is used to detect
176 whether two or more objects (usually graphical objects) collide in 3D or 2D space. Based on this concept, the sunlight
177 channel of a surface is a polygonal prism with the surface edge as the outline and the sunlight vector as the direction,
178 as shown in Fig. 2. The sunlight channel shows the maximum possible range of the source of beam irradiance received
179 by the surface at the current position of the sun. If an object either partially or entirely intersects the light channel, it

180 may have a shading effect on the target surface. Conversely, objects completely outside the sunlight channel have no
 181 shading effect on the target surface and can be screened in the shadow calculation. In addition, to further accelerate
 182 the calculation process, a hierarchical data structure was introduced. A boundary box was created for each building
 183 in the scene, which was a cuboid with the minimum rectangular boundary of the building footprint as its base and
 184 the building height as its height. The shading effect of the surrounding buildings was initially screened based on the
 185 boundary boxes before judgments at the surface level.

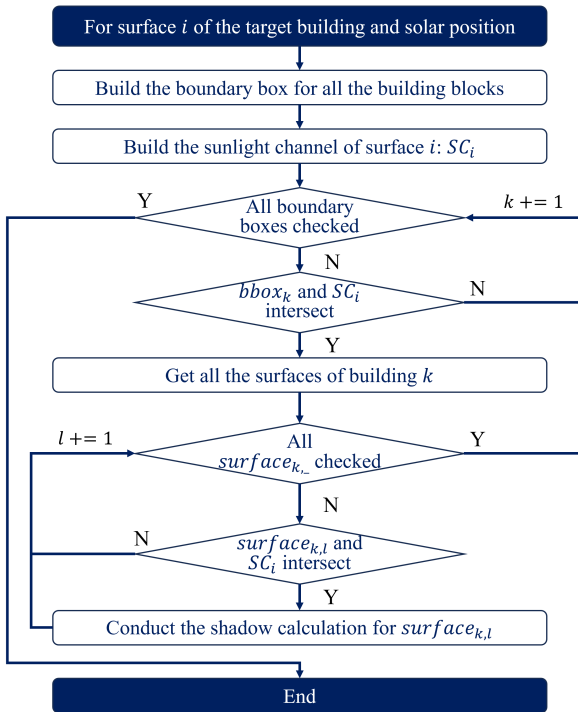


Figure 3: The main steps of the sunlight channel algorithm.

186 Fig. 3 shows the main steps of the sunlight channel algorithm. The algorithm calculates the given surface i of
 187 a target building at a certain solar position. (1) Boundary boxes were built for all building blocks. (2) The sunlight
 188 channel SC_i of surface i is built based on the outline of surface i and sunlight vector. (3) Subsequently, the intersection
 189 between the boundary box of the surrounding building and sunlight channel SC_i is determined by traversing each
 190 building in the scene. (4) If the boundary box $bbox_k$ of buildings k and SC_i do not intersect, building k will be omitted
 191 in the following calculation. Otherwise, building k may have a shading effect and should be included in the subsequent
 192 calculations. (5) To solve the shadows cast by building k , all surfaces $surface_{k,-}$ of building k are traversed. (6) If
 193 $surface_{k,l}$ does not intersect SC_i , the surface is omitted. (7) After screening, only the surfaces that could intersect SC_i
 194 remained and a shadow calculation was conducted. Based on the above steps, the shading surfaces are dynamically

195 predetermined according to the actual solar position to improve the shadow calculation process.

196 *2.2. Case studies*

197 The cases used in the comparative study are listed in Table 4. Each case was calculated using three methods to
198 assess the acceleration performance. Two building networks were used to assess the performance of the proposed
199 method compared with the existing methods, which are the hypothetical "shoe-box" buildings in a scalable neigh-
200 borhood (Building Network 1) and real buildings in a central business district (Building Network 2). For Building
201 Network 1, the number of buildings and building heights were changed to analyze the impact of spatial scale and
202 height variation.

Table 1: The cases in the comparative study.

Case No.	Building network	Number of buildings	Height entropy	Purpose
S1	Building Network 1	5×5	0	To analyze the impact of spatial scale
S2	Building Network 1	6×6	0	
S3	Building Network 1	7×7	0	
S4	Building Network 1	8×8	0	
S5	Building Network 1	9×9	0	
S6	Building Network 1	10×10	0	
H1	Building Network 1	7×7	0.14	To analyze the impact of height variation
H2	Building Network 1	7×7	0.48	
H3	Building Network 1	7×7	0.73	
H4	Building Network 1	7×7	0.86	
H5	Building Network 1	7×7	0.95	
H6	Building Network 1	7×7	0.99	
R	Building Network 2	17	2.93	To evaluate the performance in real urban contexts

203 *2.2.1. Building network 1: hypothetical "shoe-box" buildings in a scalable neighborhood*

204 A scalable neighborhood was hypothesized to compare the performance of the proposed method and existing
205 methods, and analyze the changes in model performance as the complexity of the neighborhood increases. The build-
206 ings are represented by "shoe-box" and the footprints are identical rectangles, 80m long and 50m wide. The buildings

were assumed to be south-facing, and the neighboring buildings were all spaced 13m apart. The neighborhood is located in Beijing, China.

Two extensions of the neighborhood were considered in terms of the spatial scale and height variation of the neighborhood. The spatial scale of the analysis area is related to the number of buildings and surfaces, which affect the calculation time. To analyze the impact of spatial scale on model performance, different numbers of buildings were considered. The buildings were arranged in five rows and five columns, six rows and six columns, and up to ten rows and ten columns, forming six neighborhoods with different spatial scales, that is, Cases S1 to S6. The building heights were assumed to be identical: eight stories and 24m high. The different typologies are illustrated in Fig. 4(a).

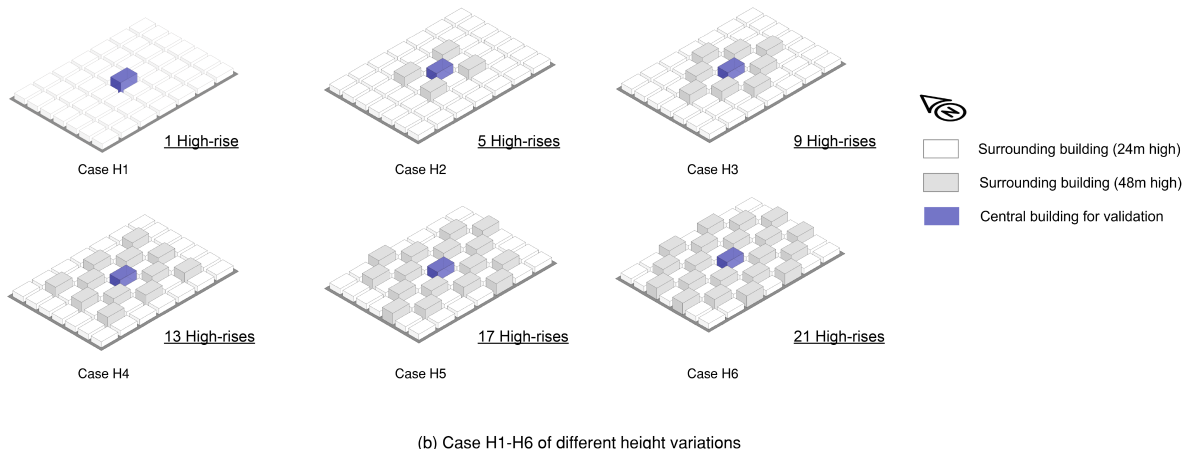
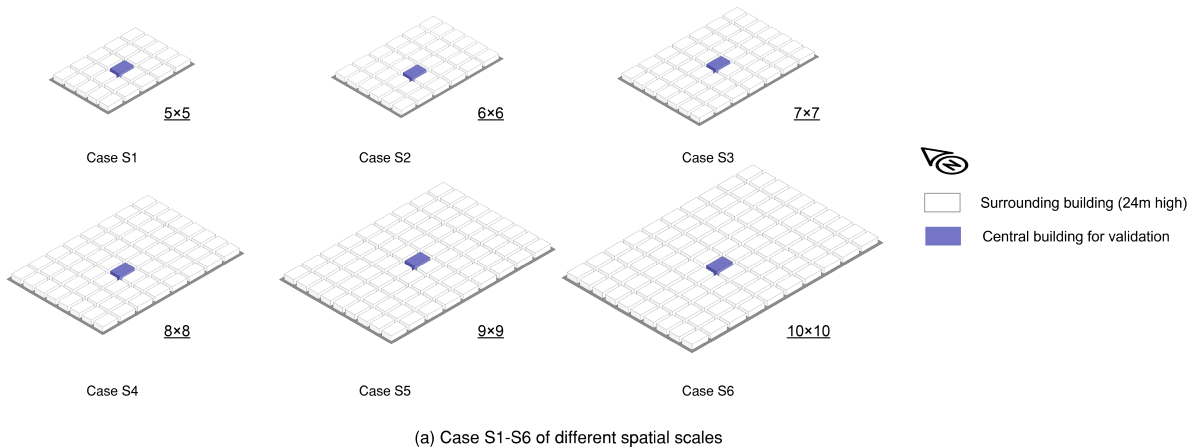


Figure 4: The cases based on Building Network 1: (a) Case S1-S6 of the different spatial scales (b) Case H1-H6 of the different height variation.

In addition to the spatial scale, height variation also affects the calculation efficiency. The more diverse the building heights in a neighborhood, the more complex the shading relationships between buildings; thus, the complexity of the calculations will increase. To analyze the impact of height variation on the model performance, six neighborhoods

218 with different levels of height variation were compared by introducing different numbers of high-rise buildings, from
 219 1 to 21, into the neighborhood with 7×7 buildings, forming Cases H1 to H6, as shown in Fig. 4(b). Each high-rise
 220 building has 16 stories and 48m high. Height entropy was introduced to quantify height variation, which represents
 221 the total diversity or disorder in building height, and is widely used as an indicator of urban morphology [44, 45].
 222 Height entropy was calculated using Eqs. 1. When the buildings in the neighborhood are the same in height, the
 223 height entropy equals 0, and if the height of each building is different, then the height entropy is the maximum. In
 224 Cases H1–H6, the height entropy increases from 0.14 to 0.99.

$$S = - \sum_{i=1}^t p_i \log_2 p_i. \quad (1)$$

225 2.2.2. Building network 2: real buildings in a central business district

226 A central business district composed of 17 buildings in Nanjing, China, was used to assess the performance of the
 227 proposed method in a real urban context, as shown in Fig. 5 (a). The neighborhood covers an area of 0.14 km^2 , with
 228 a total floor area of 0.43 km^2 . The buildings range from 2 to 45 floors, three of which are super high-rise buildings
 229 with irregularly shaped podiums and towers. The height entropy was 2.93, indicating that the height variation was
 230 more complicated than that of Building Network 1. The 3D model for the shadow calculation is shown in Fig. 5 (b),
 231 containing 836 facades and 25 roofs.

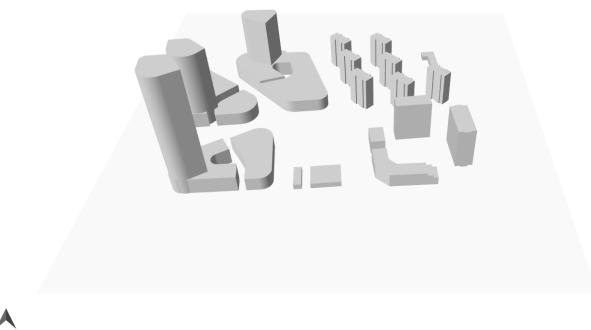


Figure 5: Buildings in a real central business district in Case R.

232 2.3. Comparative methods

233 The proposed method was compared with two other methods to assess the acceleration performance. The first
 234 is the plainest method without acceleration, where the entire model of the neighborhood is read, and the shadows
 235 between the target surface and all the other surfaces are calculated at each time step. As this method computes the
 236 entire scene for any surface, it is regarded as the ground truth for accuracy validation. The other method is the distance
 237 filtering method, which only accelerates the calculation in the surrounding environment setup by filtering the buildings

238 in the neighborhood based on their distance to the target building before the shadow calculation. After filtering, all the
239 pairs of surfaces were calculated. Owing to its wide application in UBEM, the distance filtering method was chosen
240 as the baseline to represent state-of-the-art performance.

241 The accuracy and computation time are the two main aspects of the comparative analysis. To evaluate the accuracy
242 of the different shadow calculation methods, the hourly sunlit area ratio (SAR) and total solar irradiance (G_t) on the
243 facades for the entire year were compared, which are the direct outputs of the shadow calculation models and the key
244 boundary conditions for energy modeling, respectively. The hourly calculation results were evaluated using the mean
245 absolute percentage error (MAPE). The MAPE is defined in Eqs.2, where the results of the baseline which calculates
246 shadows building by building, and surfaces by surface are regarded as the ground truth, represented as \hat{y}_i . y_i is the
247 hourly result of the three acceleration methods, distance filtering method, and proposed method. N is the total number
248 of time steps calculated, which was 8760 in the accuracy verification.

$$MAPE = 100 \times \frac{1}{N} \sum_{t=1}^N \left| \frac{y_i - \hat{y}_i}{\hat{y}_i} \right|. \quad (2)$$

249 To evaluate the accuracy of different shadow calculation methods, all three methods were programmed in C++
250 and compiled into executable files, and the computation time was counted for each case. The performance of the
251 methods was tested on a PC with an Intel(R) Core(TM) i5-12600K @3.70 GHz and 16 GB access memory (RAM).
252 The geometry of the building networks is in the format of GeoJSON, which is compatible with other UBEM and
253 GIS platforms. The building geometry was simplified to 2.5D blocks by removing details such as sloping roofs and
254 setbacks with increasing tower height.

255 **3. Results**

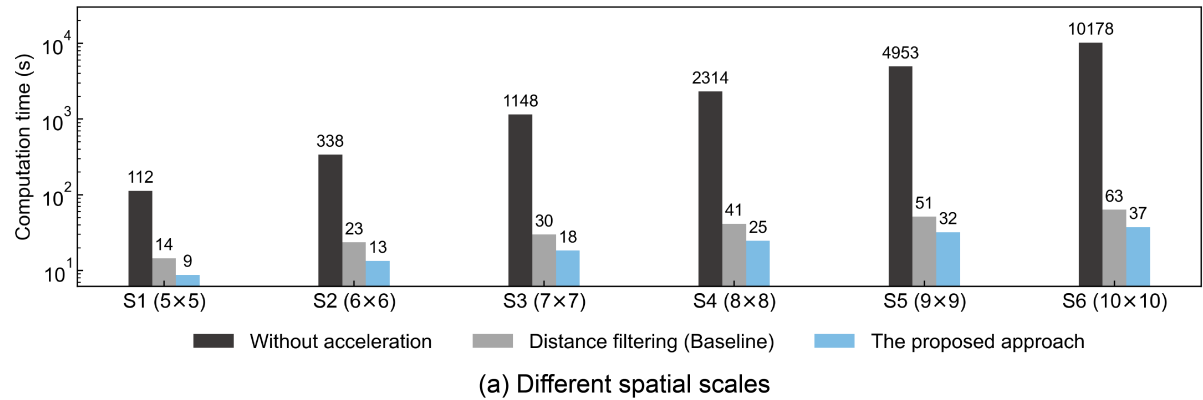
256 *3.1. Computation intensity analysis*

257 *3.1.1. The impact of spatial scale*

258 The computation times for the different spatial scales were analyzed, as shown in Fig. 6(a). As the spatial scale
259 of the neighborhood increases, the calculation time also increases. In the proposed method, the computation time
260 increases from 8.73s to 37.37s, while in the distance filtering method (baseline), it varies between 14.48s and 63.49s.
261 Despite the small size of this case, a significant acceleration has been achieved by the acceleration methods. The
262 computation time of the proposed method was significantly shorter than that of the non-accelerated method, and it
263 outperformed the baseline in terms of efficiency. This is because the sunlight channel algorithm filters the surfaces
264 based on the variable sun position, further reducing the number of calculations required by the distance filtering

265 method.

266 Comparing the computation time as the spatial scale increases, the computation time of the non-accelerated
267 method increases dramatically by more than 89 times, whereas the computation time of the other two acceleration
268 methods increases much more moderately, as shown in Fig. 6(a). Specifically, the distance filtering method (baseline)
269 increased by 3.5 times and the proposed method only increased by 3.1 times. In the non-accelerated method, as the
270 number of buildings to be calculated increased, the number of surfaces also increased, leading to an accelerated in-
271 crease in the computation time. However, for the baseline and proposed methods, the scene for shadow calculation is
272 limited to a certain distance from the target building, and for the proposed method, the surfaces outside the sunlight
273 channel are filtered out, which means that the required number of calculations will not increase as the spatial scale of
274 the whole neighborhood increases.



(a) Different spatial scales

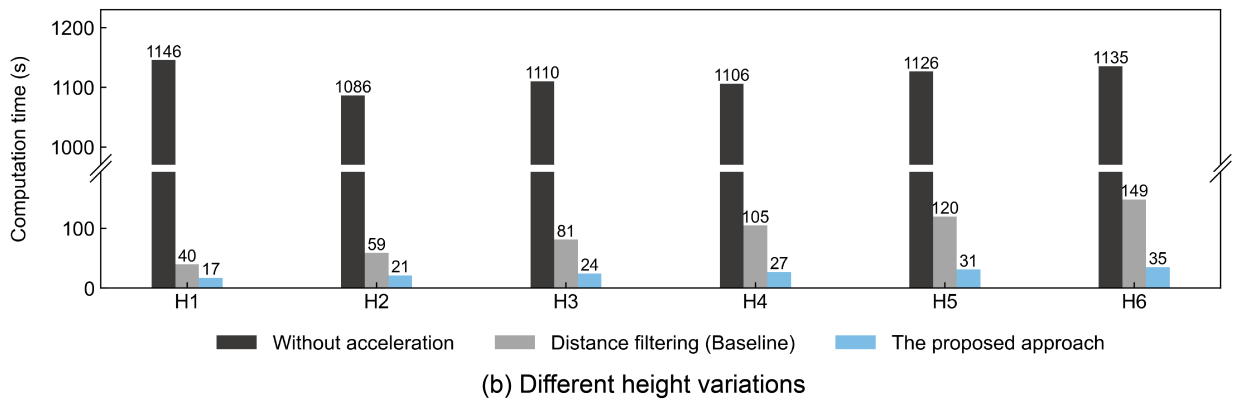


Figure 6: Computation time for different methods: (a) with increasing spatial scale and (b) with increasing height variation.

275 Compared with the non-accelerated method, the proposed method and the baseline can both better cope with the
276 growth of the computation time on a spatial scale, since the shading scene for each target building after distance
277 filtering is significantly pruned and quite similar in neighborhoods with regular buildings of different spatial scales.

278 The proposed method can further accelerate the calculation compared to the baseline because the sunlight channel
279 algorithm can further reduce the number of surfaces to be calculated. The proposed method combines the strengths of
280 both the distance filtering and sunlight channel methods, which can solve the problem of a sharp increase in shadow
281 computation time when the spatial scale increases.

282 *3.1.2. The impact of height variation*

283 Fig. 6(b) shows the computation time of the neighborhoods with different height variations. In this case, the
284 number of high-rise buildings increased, and the spatial scale of the neighborhood remained the same. The computa-
285 tion times of the distance filtering method (baseline) and proposed method increased as the level of height variation
286 increased. Specifically, the computation time of the proposed method increases from 17.38s to 35.06s, while in the
287 distance filtering method, it increases from 39.77s to 148.62s.

288 The computation time of the proposed method was slightly higher than that of the baseline method. As the level
289 of height variation increases in the neighborhood, more buildings are recognized as having a shading effect on the
290 distance filtering. The acceleration of the distance filtering method is less effective because fewer buildings are filtered
291 out. However, the proposed method performs much better because it filters surfaces based on sunlight and relative
292 building positions and can still provide good filtration for neighborhoods with large height variations. Therefore, the
293 sunlight channel algorithm combined with distance filtering can cope better with the increase in computation time
294 with height variations.

295 The calculation in the proposed method was accelerated by more than 31 times compared to the non-accelerated
296 method, whereas the baseline accelerated the computation speed by less than seven times for the neighborhood with
297 the greatest height variation. Therefore, for neighborhoods with large variations in building height, the proposed
298 method of combining sunlight channels and distance filtering is more efficient.

299 A comparison of the trends in the computation time in Fig.6(a) and (b), the computation time of the baseline is
300 less affected by height variation, different from the impact of spatial scale, since the numbers of buildings in Case
301 H1-H6 are the same and the number of buildings in Case S1-S6 grows quadratically. The computation time of the
302 distance filtering method (baseline) was more sensitive to the height variation than to the spatial scale. In Case S1-S6
303 of different spatial scales, the shading scene of each building is similar owing to the identical heights of the buildings,
304 whereas the shading scenes become more complicated as the levels of height variation increase from Case H1 to H6,
305 which results in a weakening of the acceleration effect of distance filtering.

306 3.2. Accuracy verification

307 The central building of each neighborhood in Building Network 1 was selected as a validation case, as the dark
 308 buildings shown in Fig.4. The neighborhoods of six spatial scales and six height variations were validated to ensure
 309 the accuracy of the acceleration methods.

310 3.2.1. Different spatial scales

311 Fig.7 shows the MAPEs of the sunlit area ratios of the central building's facades in the neighborhoods of different
 312 spatial scales. The results of the proposed method and the baseline are the same, which means that the errors in
 313 the sunlit area ratio are mainly caused by the surrounding environment setup caused by distance filtering. Once
 314 the surrounding environment is finalized, the sunlight channel method has no impact on the accuracy of the shadow
 315 calculation process, which only filters surfaces without shading effects. Therefore, the accuracy of the proposed
 316 method depends on the distance threshold in the distance filtering.

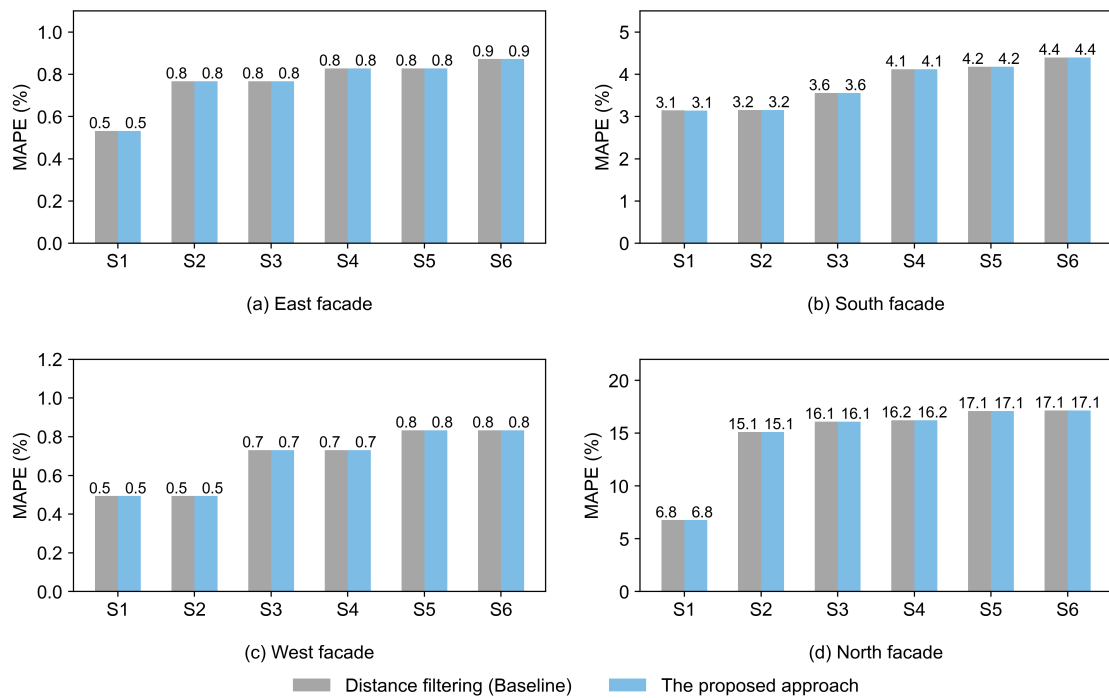


Figure 7: MAPEs of the sunlit area ratios (SARs) of the central building's facades in Case S1-S6 of different spatial scales.

317 Regarding the errors in SARs for different facades introduced by distance filtering, the north facade had the largest
 318 MAPEs, between 6.8% and 17.1%. Following this, the MAPEs of the south facade were also large, ranging from
 319 3.1% to 4.4%. The east and west facades had the best accuracy with the MAPEs below 0.9%. The errors of the SARs
 320 increase with an increase in spatial scale because the numbers of filtered buildings are the same for the neighborhoods

321 in S1-S6, where the building heights are identical. As the spatial scale increased, more surrounding buildings were
 322 filtered out; therefore, more surfaces that may have shading effects were not accounted for.

323 The accuracy of the total solar irradiance of each facade was compared as shown in Fig. 8. The north facade has
 324 the largest MAPEs in the distance filtering process, between 0.20% and 0.25%, followed by the south facade, which
 325 is between 0.09% and 0.16%. The MAPEs of the east facade and west facade were much smaller, both below 0.07%.
 326 However, compared with the results shown in Fig. 7, the MAPEs of the total irradiance are much lower than those of
 327 the sunlit area ratio. Therefore, the proposed method performed well for calculating the total irradiance.

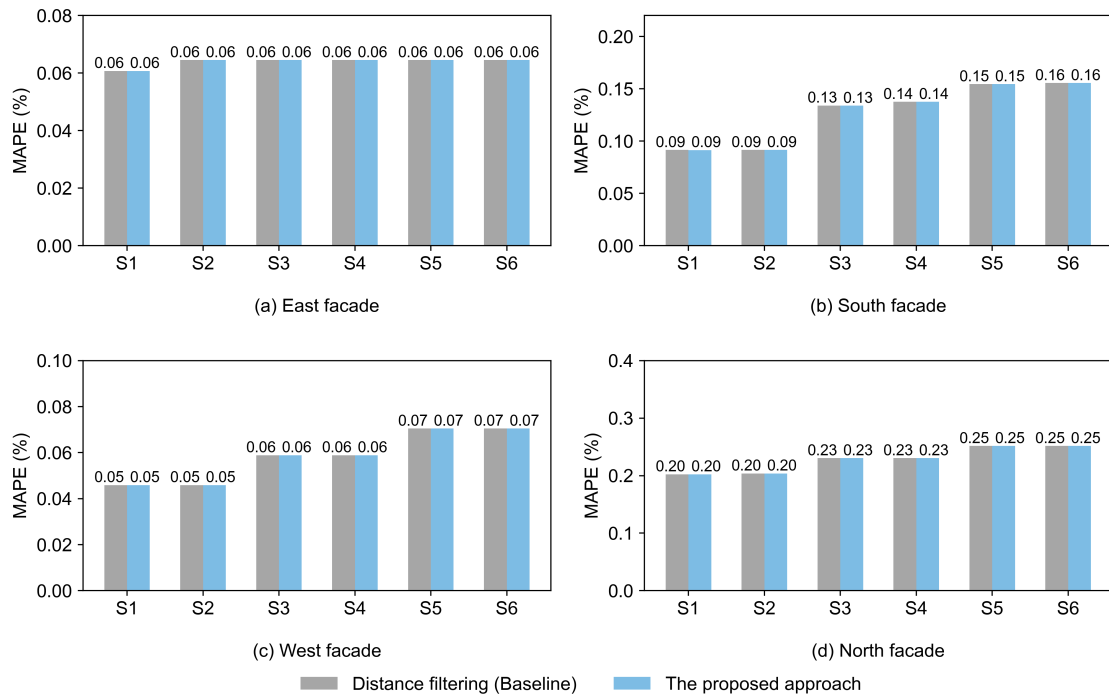


Figure 8: MAPEs of the total irradiance of the central building's facades in Case S1-S6 of different spatial scales.

328 3.2.2. Different height variations

329 Fig. 9 shows the MAPEs of the sunlit area ratios of the central building's facades in the neighborhoods of different
 330 height variations. As shown by the same error results between the proposed method and the baseline, the sunlight
 331 channel itself does not introduce errors, whereas distance filtering does. The north facade has the largest MAPEs
 332 between 2.2% and 31.1%, similar to the results of the neighborhoods with different spatial scales. The errors in the
 333 east and west facades were similar, with MAPEs of 9.0% and 10.6% for Case H6 with the highest level of height
 334 variation, respectively. The MAPE of the south facade in Case H6 was 4.5%.

335 Comparing the accuracy of different levels of height variation, the MAPEs increased significantly in Cases H5 and
 336 H6 when the height variation of the neighborhood was complicated to a certain degree. This is because the outermost

337 high-rise buildings to the east and west were screened out by distance filtering in Cases H5 and H6; however, they still
 338 had shading effects on the target building. Although the distance between the centroid of the surrounding building
 339 and that of the target building is greater than the threshold, there may still be occlusion between the building surfaces
 340 because the distance between the surfaces may be less than the distance between the centroids of the two buildings.

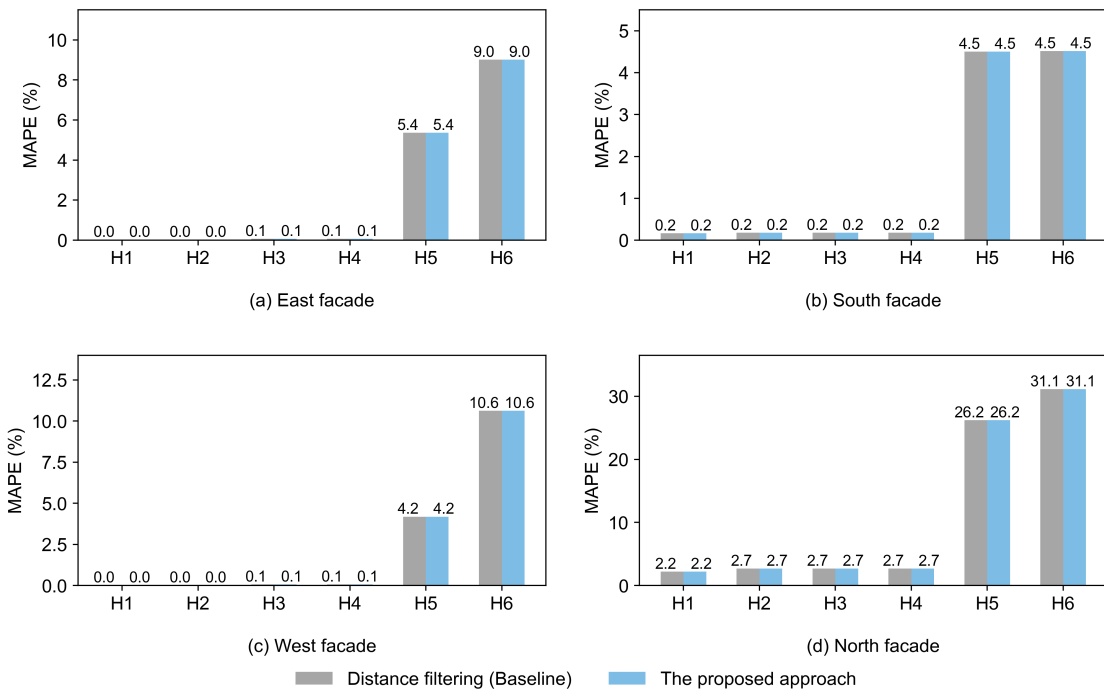


Figure 9: MAPEs of the sunlit area ratios (SARs) of the central building's facades in Case H1-H6 of different height variations.

341 Fig. 10 showed the errors in the total solar irradiance of each facade. The west facade has the largest MAPEs of
 342 the total irradiance among all the other facades, although the MAPE of SAR for the west facade is not the largest.
 343 For Case H6, which had the highest level of height variation, the MAPE of the total solar irradiance for the west
 344 facade was 1.59%. The MAPEs of the east facade in Case H6 was 0.65%. In comparison, the accuracies of the south
 345 and north facades were higher, with maximum MAPEs of 0.16% and 0.36%, respectively. In general, the proposed
 346 method can calculate the solar irradiance of the facades accurately.

347 3.3. Application in the real building network

348 Different methods have been applied to build networks in the central business district. The performance of the
 349 proposed method was compared with that of the distance filtering method (baseline) and non-accelerated method
 350 (ground truth) in terms of accuracy and computation time.

351 Fig. 11 shows the hourly solar radiation aggregated by all the building surfaces in the neighborhood. Jan.15th,
 352 Apr.15th, Jul.15th, and Oct.15th were selected as typical days to evaluate the accuracy of the different methods. The

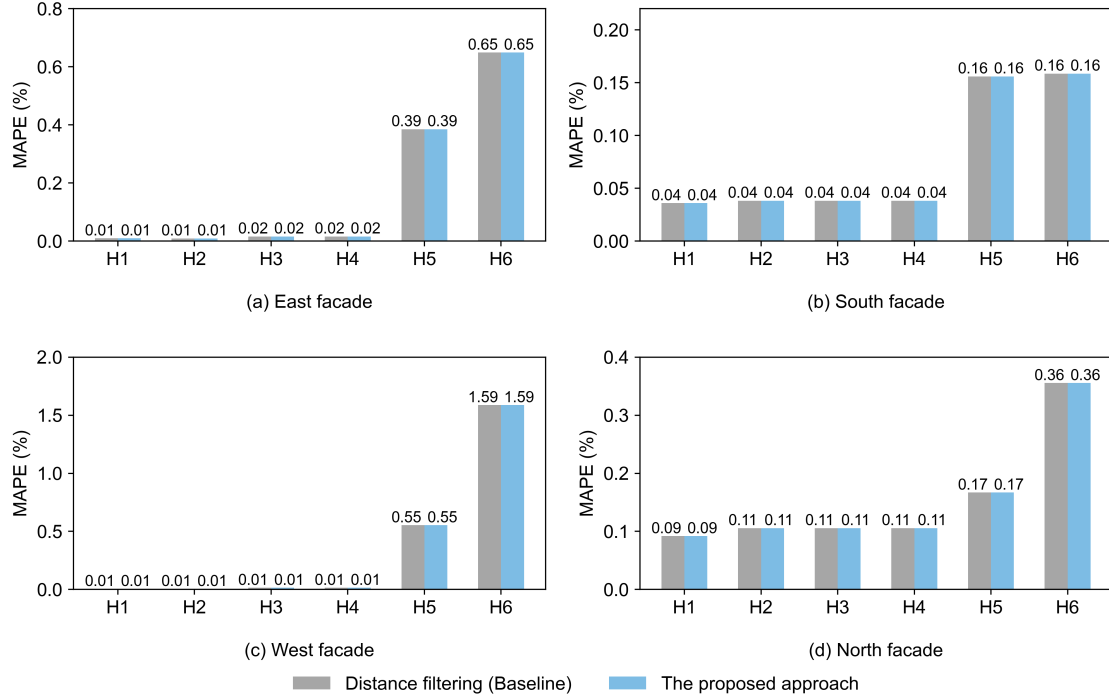


Figure 10: MAPEs of the total irradiance of the central building's facades in Case H1-H6 of different height variations.

353 proposed method has very small errors, which indicates that the errors of the proposed method are acceptable when
354 applied to a real urban building network.

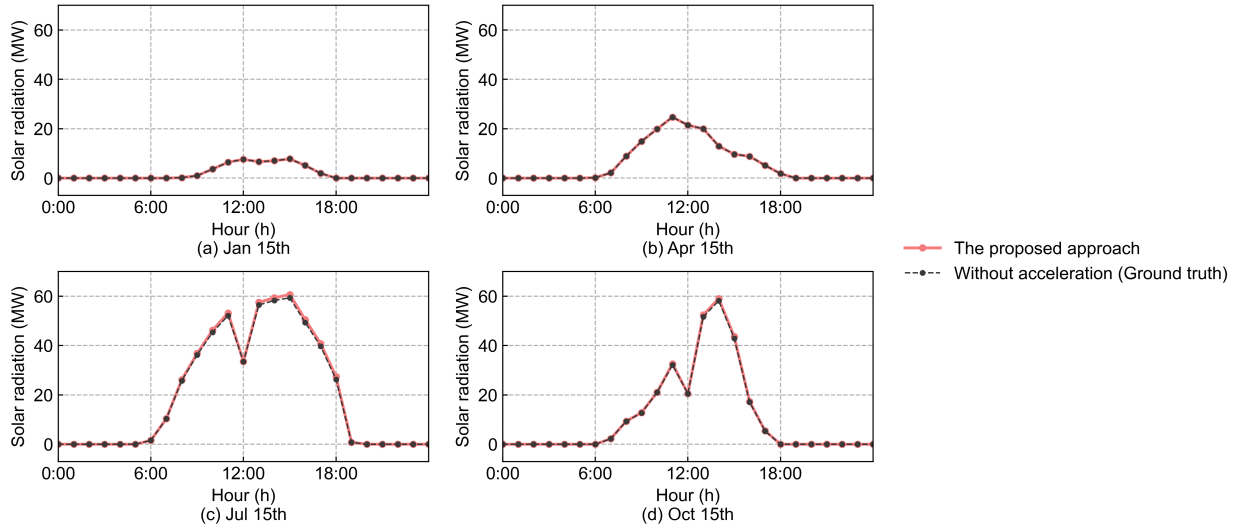


Figure 11: The hourly solar radiation aggregated by all the building surfaces on (a) Jan. 15th, (b) Apr. 15th, (c) Jul. 15th, and (d) Oct. 15th.

355 The MAPEs of the hourly solar radiation calculated using the different methods are listed in Table 2. The MAPE
356 of the proposed method is below 1.2%, which shows that the acceleration methods have good accuracy in terms of

357 the total solar radiation. In addition, the proposed method had the same MAPE as the baseline. Table 3 compares the
 358 annual total solar radiation obtained using different methods. The proposed method and the baseline both overesti-
 359 mated the total solar radiation by 1.87% because the distance filtering process may have filtered some surfaces that
 360 shaded the target building when the solar altitude was low. This indicates that the proposed method can provide a
 361 good estimation of the total annual solar radiation.

Table 2: MAPEs of the total solar radiation for different methods.

	Distance filtering (Baseline)	The proposed method
MAPE of total solar radiation (%)	1.13	1.13

362 Fig. 12 shows the computation time of the different methods. The computation time is much longer than that in
 363 the cases using Building Network 1, owing to the more irregular building footprints and steeper changes in building
 364 heights. The computation time of the non-accelerated method is up to 19768.74s (5.49h), which makes it difficult to
 365 apply shadow calculations for energy analysis. The total computation time of the proposed method was only 551.57s,
 366 which was only 2.8% of the computation time of the non-accelerated method. However, the distance filtering method
 367 (baseline) takes 6087.05s (1.69h), which is more than 11 times than the proposed method. Therefore, for complex
 368 urban building networks, the proposed method can further unlock the acceleration potential compared with using only
 369 distance filtering.

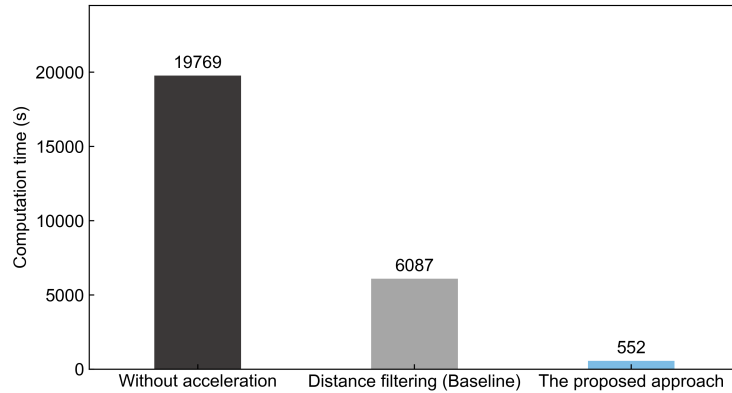


Figure 12: Computation time for different methods in Case R of Building Network 2.

Table 3: Annual total solar radiation for different methods.

	Ground truth	Distance filtering (Baseline)	The proposed method
Annual total solar radiation (GWh)	107	109	109

370 **4. Discussion**

371 *4.1. Further analysis of error and temporal characteristics*

372 The cases with the largest errors in the total irradiance, the north facade in Case S6 and the west facade in Case
373 H6, were taken as examples to analyze the calculation errors and temporal characteristics.

374 The errors in the north facade in Case S6 are shown in Fig. 13. The errors throughout the year were mainly
375 found in March and April, when the north facade was exposed to beam radiation and the solar altitude was low, as
376 shown in Fig. 13(a). The week with high errors was further analyzed, as shown in Fig. 13(b). The errors occurred
377 mainly at 6:00 and 18:00 throughout the day, which coincided with the sunrise and sunset times during this period.
378 In the distance filtering process, surfaces that cast shadows when the solar altitude is below 10° are excluded from
379 the scene for shadow calculation, leading to errors immediately after sunrise or before sunset. March 27th was taken
380 as an example to analyze the error in the sunlit area ratio and total solar irradiance, as shown in Fig. 13 (c) and (d).
381 Although there may have been large differences in SARs at sunrise and sunset, the differences in the total radiation
382 were almost negligible. The solar irradiance is weak at sunrise and sunset times of the day, and therefore, the large
383 errors in SARs are not propagated to the total solar irradiance.

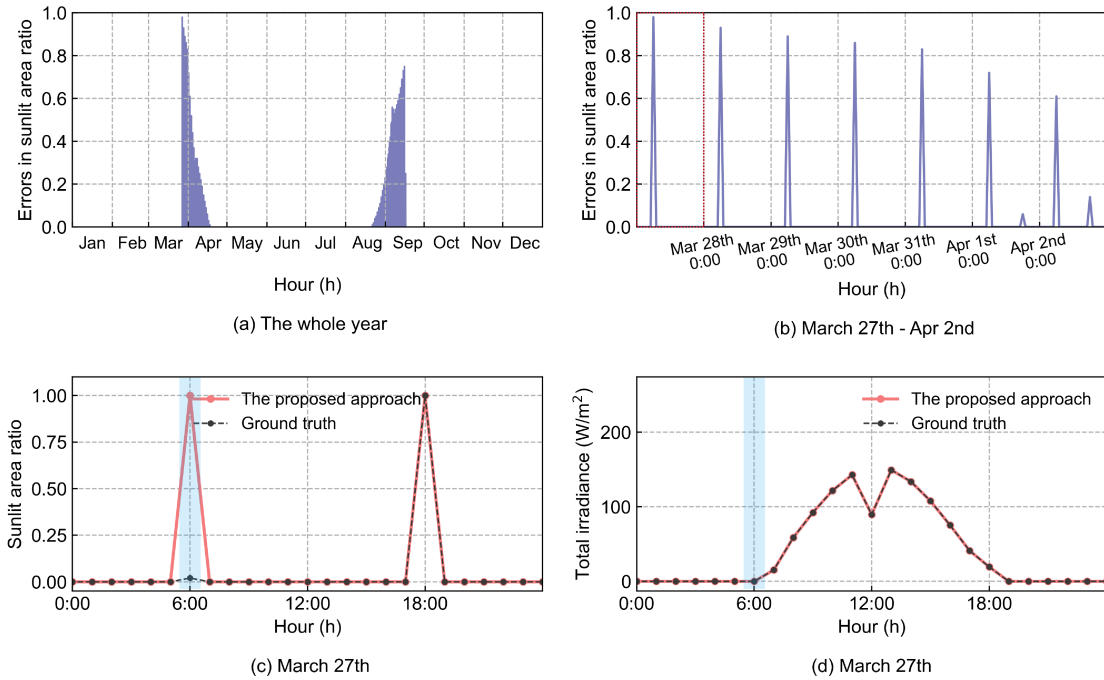


Figure 13: Error analysis of the north facade of the central building in Case S6: Difference in SAR between the proposed method and the ground truth (a) in the whole year, (b) in the typical week, (c) on a typical day, and (d) the total irradiance on a typical day.

384 The errors of the west facade in Case H6 are shown in Fig. 14. The MAPEs of SARs are much lower than those
385 of the total solar irradiance. First, the SAR mainly affects the direct irradiance, whereas the diffuse irradiance and

386 reflected irradiance are also accounted for in the total solar irradiance. Another reason is that the solar radiation is
 387 low when there are errors in SARs. As shown in Fig. 14(a), the errors in SAR occur in most time of the whole year,
 388 while the absolute errors are all below 0.2. The time of occurrence of the errors for the west facade is different from
 389 that for the north facade because the west facade receives direct solar radiation for most of the year. As shown in Fig.
 390 14(b), the errors in SARs occur at 19:00 throughout the day, which is the time of sunset in this period. Similar to the
 391 analysis of the north facade in Fig. 13(b), the error is introduced by distance filtering when the sunlight comes from
 392 the west and the altitude angle is below the threshold. On a typical day (May 9th), as shown in Fig. 14(c) and (d), the
 393 proposed method may overestimate the sunlit area ratio of the west facade at sunset due to neglecting some shading
 394 surfaces, while the difference in the total irradiance is small.

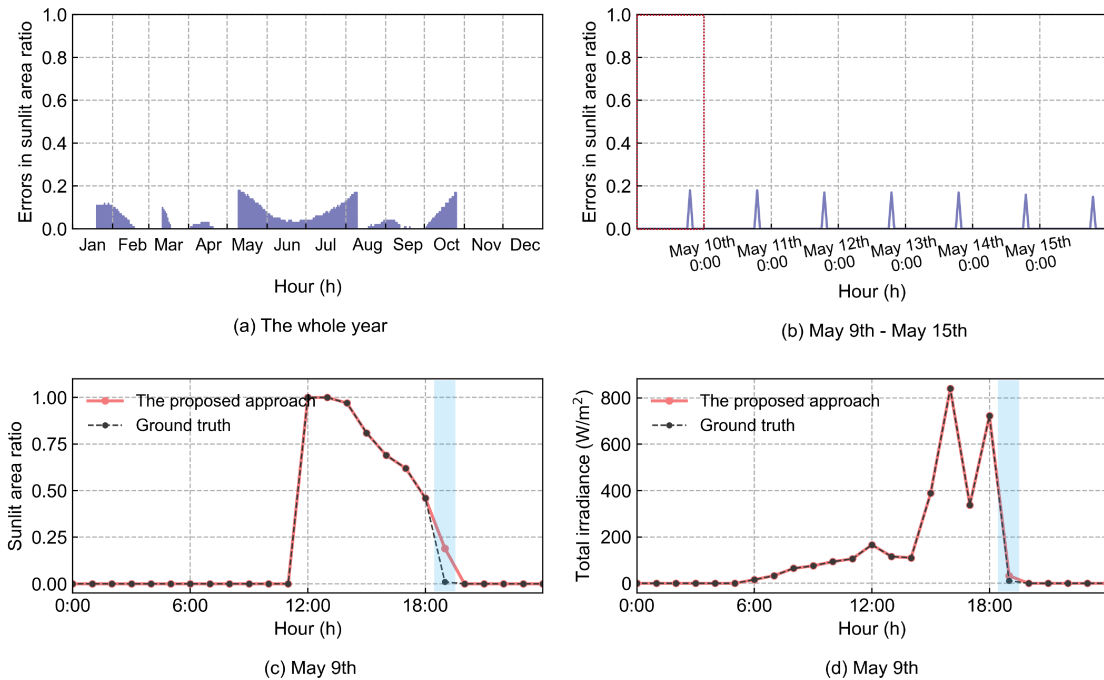


Figure 14: Error analysis of the west facade of the central building in Case H6: Difference in SAR between the proposed method and the ground truth (a) in the whole year, (b) in the typical week, (c) on a typical day, and (d) the total irradiance on a typical day.

395 4.2. Comparison of the proposed method and the baseline

396 Based on the above analyses, distance filtering and sunlight channels focus on different aspects of the acceleration
 397 of the shadow calculation, and the integrated method shows great acceleration potential. The sunlight channel is an
 398 algorithm without error. Therefore, the proposed method yields almost the same results as the baseline, except for
 399 the numerical errors due to the finite precision of computations or truncation errors, which could be acceptable for
 400 engineering applications. Whereas distance filtering introduces errors in the surrounding environment setup. When

401 the solar altitude was below the threshold, shadows cast by some surfaces were ignored during distance filtering. In
 402 addition, distance filtering was based on the Euclidean distance between the centroids of the buildings. For buildings
 403 with large footprints or irregular shapes, this criterion may ignore shading effects on certain surfaces [42].

404 Regarding computational efficiency, integrating sunlight channel techniques on top of distance filtering can further
 405 increase the calculation speed; however, the performance improvement varies in different cases. Fig. 15 summarized
 406 the acceleration multipliers of the proposed method over the baseline in different cases. As the spatial scale increased
 407 in Case S1-S6, the acceleration multipliers of the proposed method were similar, between 56% and 77%. As the
 408 height variation increased in Case H1-H6, the acceleration multipliers of the proposed method became significantly
 409 greater than those in Case S1-S6. The acceleration multiplier increased from 1.35 to 3.26. Therefore, the proposed
 410 method performed better in neighborhoods with complex changes in building heights.

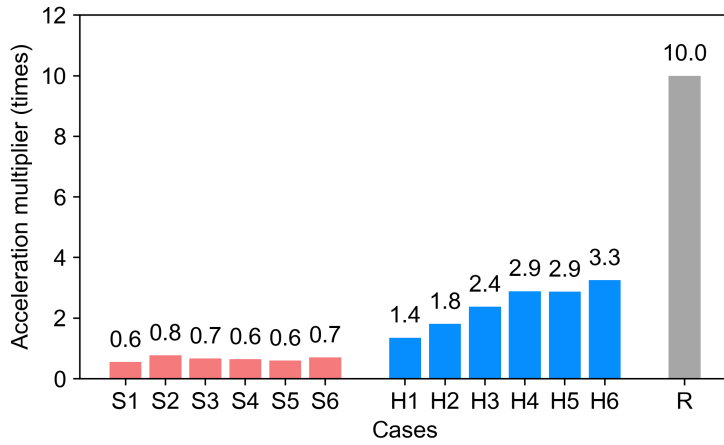


Figure 15: The acceleration multipliers of the proposed method over the baseline in different cases.

411 For real urban buildings in Case R, the acceleration multiplier of the proposed method reached 10.0, which means
 412 that the distance filtering method alone may not be sufficient for complex urban environments. The geometries of the
 413 real urban buildings in Building Network 2 are more complicated than those of the "shoe-box" buildings in Building
 414 Network 1, where the building facades consist of a large number of small facades. At the baseline, the buildings (or
 415 surfaces) were screened by neglecting specific sun positions; therefore, the number of small facades to be calculated
 416 could not be minimized. In the proposed method, only the surfaces in the sunlight channel of a specific sun position
 417 can be calculated. Thus, the amount of computation is further reduced after distance filtering. However, establishing
 418 sunlight channels and determining the relative position of surrounding surfaces to the sunlight channels increases the
 419 amount of computation. Therefore, a trade-off needs to be made between the additional computational effort brought
 420 by the sunlight channel and the filtering of the surfaces to be computed. If there are few buildings around the target
 421 building and the sunlight channel does not filter the surfaces, the proposed method may not be as effective as the

422 conventional method. In urban areas with high building densities, the sunlight channel algorithm can significantly
423 reduce the computational effort with only a small amount of pre-determination, outperforming traditional methods in
424 most cases. In summary, the proposed method integrating distance filtering and sunlight channels can cope well with
425 both the large-scale urban model and the complexity of building structures, and shows good performance in shadow
426 calculation in UBEM.

427 In addition, although the building models in building network 2 are single-zone models, the proposed method
428 will further outperform the baseline method for models with more complex structure or higher levels of detail. With
429 more detailed floor configurations and finer division of surface patches, the building surfaces will be divided into
430 more patches. On the one hand, smaller building surface patches will reduce the size of sunlight channels, and more
431 surrounding surfaces will be filtered out, all of which will be calculated in the baseline. On the other hand, more
432 surface patches will increase the amount of computation, as both the surface patches and the surrounding surfaces
433 to be calculated will increase. Therefore, the advantage of the proposed method over the baseline will be more
434 pronounced for building models with higher levels of detail.

435 4.3. *Integration with UBEM tools*

436 The proposed sunlight-channel-based method in this study is an efficient approach for the inter-building shadow
437 calculation in the urban context. The shadow calculation module has been programmed and integrated into DeST-
438 urban, the UBEM platform based on DeST. Specifically, the shadow calculation module calculates the SAR of each
439 building surface based on geometric information and configures it in the BEM. The simulation engine (DeST) will
440 use these SARs to calculate the solar heat gain without including the surrounding surfaces into the BEM. Therefore,
441 the performance simulation for each building will be decoupled after the SARs are calculated.

442 4.4. *Potential further investigations*

443 Although this study proposed an integrated method for shadow calculation in UBEM and had good performance
444 in terms of accuracy and efficiency, there are some potential further investigations. The first step is the determination
445 of the distance threshold in distance filtering. A larger distance threshold improves the accuracy, but the calculation
446 process may slow down. Although the distance threshold selected in this study showed high accuracy for the total
447 solar irradiance of building surfaces, a proper distance threshold will further balance the accuracy and computation
448 efficiency.

449 The second is the parallelization of the shadow calculation. After distance filtering, the complex shading rela-
450 tionships among the buildings were decoupled into a shading scene for each building, which was suitable for parallel

451 computing. Novel parallel algorithms can further reduce the running time of large-scale shadow calculations [46].
452 Additionally, the use of graphics processing units (GPUs) is a promising acceleration approach [47, 48].

453 **5. Conclusion**

454 In this study, a sunlight channel algorithm was proposed to dynamically predetermine shading surfaces to further
455 accelerate the shadow calculation process. Based on the sunlight channel, a novel acceleration approach for calculating
456 shadows for urban building energy modeling was proposed. The main findings of this study are as follows:

- 457 • The proposed approach could decrease computation time significantly. For Building Network 1, the proposed
458 approach could accelerate the calculation process by 70% over the baseline in the case with the largest spatial
459 scale, and 3.3 times over the baseline in the case with the highest level of height variation. The acceleration
460 effect of the proposed method is more significant in neighborhoods with complex changes in building heights.
461 The proposed approach can cope well with both the large-scale urban model and the complexity of the building
462 structures.
- 463 • The proposed approach could achieve high accuracy in calculating the sunlit area ratio and total solar radiation
464 of building surfaces. In the case studies of Building Network 1, the MAPEs of SARs and total solar radiations
465 are all below 31.1% and 1.59%, respectively. Distance filtering is the reason for the calculation errors depending
466 on the distance threshold in distance filtering, while the sunlight channel itself has no impact on the accuracy of
467 the shadow calculation process.
- 468 • The proposed approach showed good accuracy and acceleration performance in applications on real urban build-
469 ing networks. The MAPE of total solar radiation is only 1.13% compared to the ground truth. The computation
470 speed of the proposed approach is increased by more than 10 times over the baseline.

471 The work presented in this paper makes it possible to calculate shadows with high fidelity and efficiency in com-
472 plex urban environments. The proposed approach supports an accurate and rapid analysis of the energy consumption
473 and solar potential of buildings, thus providing quantitative tools for optimal design and decision-making in urban
474 environments.

475 **Acknowledgements**

476 This study was supported by the National Natural Science Foundation of China (Grant Number: 52225801) and
477 Beijing Municipal Natural Science Foundation of China (Grant number 8222019).

478 **References**

- 479 [1] IEA, Empowering Cities for a Net Zero Future: Unlocking Resilient, Smart, Sustainable Urban Energy Systems, OECD Publishing, 2021.
- 480 [2] D. Yan, X. Zhou, J. An, X. Kang, F. Bu, Y. Chen, Y. Pan, Y. Gao, Q. Zhang, H. Zhou, et al., DeST 3.0: A new-generation building performance
481 simulation platform, *Building Simulation*.
- 482 [3] P. Wang, Z. Liu, L. Zhang, Sustainability of compact cities: A review of inter-building effect on building energy and solar energy use,
483 *Sustainable Cities and Society* 72 (2021) 103035.
- 484 [4] T. Hong, Y. Chen, X. Luo, N. Luo, S. H. Lee, Ten questions on urban building energy modeling, *Building and Environment* 168 (2020)
485 106508.
- 486 [5] X. Shen, H. Liu, X. Yang, X. Zhou, J. An, D. Yan, A data-mining-based novel approach to analyze the impact of the characteristics of urban
487 ventilation corridors on cooling effect, *Buildings* 14 (2) (2024) 348.
- 488 [6] A. L. Pisello, J. E. Taylor, X. Xu, F. Cotana, Inter-building effect: Simulating the impact of a network of buildings on the accuracy of building
489 energy performance predictions, *Building and environment* 58 (2012) 37–45.
- 490 [7] H. Liu, Y. Pan, Y. Yang, Z. Huang, Evaluating the impact of shading from surrounding buildings on heating/cooling energy demands of
491 different community forms, *Building and Environment* 206 (2021) 108322.
- 492 [8] B. Xia, Z. Li, Optimization of residential urban-block morphology based on its synthetic effects on indoor and outdoor natural lighting
493 environments, *Sustainable Cities and Society* (2023) 104698.
- 494 [9] H. Ren, C. Xu, Z. Ma, Y. Sun, A novel 3d-geographic information system and deep learning integrated approach for high-accuracy building
495 rooftop solar energy potential characterization of high-density cities, *Applied Energy* 306 (2022) 117985.
- 496 [10] Z. Ren, Y. Chen, C. Song, M. Liu, A. Xu, Q. Zhang, Economic analysis of rooftop photovoltaics system under different shadowing conditions
497 for 20 cities in china, *Building Simulation* 17 (2) (2023) 235252. doi:10.1007/s12273-023-1082-5.
- 498 [11] S.-Y. Li, J.-Y. Han, The impact of shadow covering on the rooftop solar photovoltaic system for evaluating self-sufficiency rate in the concept
499 of nearly zero energy building, *Sustainable Cities and Society* 80 (2022) 103821.
- 500 [12] U. Ali, M. H. Shamsi, C. Hoare, E. Mangina, J. O'Donnell, Review of urban building energy modeling (ubem) approaches, methods and tools
501 using qualitative and quantitative analysis, *Energy and buildings* 246 (2021) 111073.
- 502 [13] Z. Liu, Z. Dou, H. Chen, C. Zhang, S. Wang, Y. Wu, X. Liu, D. Yan, Exploring the impacts of heterogeneity and stochasticity in air-
503 conditioning behavior on urban building energy models, *Sustainable Cities and Society* (2024) 105285.
- 504 [14] F. Johari, G. Peronato, P. Sadeghian, X. Zhao, J. Widén, Urban building energy modeling: State of the art and future prospects, *Renewable
505 and Sustainable Energy Reviews* 128 (2020) 109902.
- 506 [15] Z. Liu, X. Zhou, W. Tian, X. Liu, D. Yan, Impacts of uncertainty in building envelope thermal transmittance on heating/cooling demand in
507 the urban context, *Energy and Buildings* 273 (2022) 112363.
- 508 [16] Z. Deng, Y. Chen, J. Yang, Z. Chen, Archetype identification and urban building energy modeling for city-scale buildings based on gis
509 datasets, *Building Simulation* 15 (9) (2022) 15471559. doi:10.1007/s12273-021-0878-4.
- 510 [17] Z. Deng, K. Javanroodi, V. M. Nik, Y. Chen, Using urban building energy modeling to quantify the energy performance of residential buildings
511 under climate change, *Building Simulation* 16 (9) (2023) 16291643. doi:10.1007/s12273-023-1032-2.
- 512 [18] J. T. Szcześniak, Y. Q. Ang, S. Letellier-Duchesne, C. F. Reinhart, A method for using street view imagery to auto-extract window-to-wall
513 ratios and its relevance for urban-level daylighting and energy simulations, *Building and Environment* 207 (2022) 108108.
- 514 [19] R. Zhu, M. S. Wong, L. You, P. Santi, J. Nichol, H. C. Ho, L. Lu, C. Ratti, The effect of urban morphology on the solar capacity of
515 three-dimensional cities, *Renewable Energy* 153 (2020) 1111–1126.

- 516 [20] Y. Chen, T. Hong, M. A. Piette, Automatic generation and simulation of urban building energy models based on city datasets for city-scale
517 building retrofit analysis, *Applied Energy* 205 (2017) 323–335.
- 518 [21] Y. Etzion, An improved solar shading design tool, *Building and Environment* 27 (3) (1992) 297–303.
- 519 [22] B. Decker, U. Jahn, Performance of 170 grid connected pv plants in northern germanyanalysis of yields and optimization potentials, *Solar*
520 *Energy* 59 (4-6) (1997) 127–133.
- 521 [23] N. L. Jones, D. P. Greenberg, K. B. Pratt, Fast computer graphics techniques for calculating direct solar radiation on complex building
522 surfaces, *Journal of Building Performance Simulation* 5 (5) (2012) 300–312.
- 523 [24] A. P. de Almeida Rocha, G. Reynoso-Meza, R. C. Oliveira, N. Mendes, A pixel counting based method for designing shading devices in
524 buildings considering energy efficiency, daylight use and fading protection, *Applied Energy* 262 (2020) 114497.
- 525 [25] G. J. Ward, The radiance lighting simulation and rendering system, in: *Proceedings of the 21st annual conference on Computer graphics and*
526 *interactive techniques*, 1994, pp. 459–472.
- 527 [26] A. Vulkan, I. Kloog, M. Dorman, E. Erell, Modeling the potential for pv installation in residential buildings in dense urban areas, *Energy and*
528 *Buildings* 169 (2018) 97–109.
- 529 [27] K. Shono, Y. Yamaguchi, U. Perwez, T. Ma, Y. Dai, Y. Shimoda, Large-scale building-integrated photovoltaics installation on building
530 façades: Hourly resolution analysis using commercial building stock in tokyo, japan, *Solar Energy* 253 (2023) 137–153.
- 531 [28] A. Yezioro, E. Shaviv, Shading: A design tool for analyzing mutual shading between buildings, *Solar Energy* 52 (1) (1994) 27–37. doi:
532 [10.1016/0038-092x\(94\)90078-g](https://doi.org/10.1016/0038-092x(94)90078-g).
- 533 [29] J. Hoover, T. Dogan, Fast and robust external solar shading calculations using the pixel counting algorithm with transparency, in: *Building*
534 *Simulation Conference Proceedings, IBPSA*, 2017. doi:[10.26868/25222708.2017.287](https://doi.org/10.26868/25222708.2017.287).
- 535 [30] F. Zhang, H. Sun, L. Xu, L. K. Lun, Parallel-split shadow maps for large-scale virtual environments, in: *Proceedings of the 2006 ACM*
536 *international conference on Virtual reality continuum and its applications*, 2006, pp. 311–318.
- 537 [31] J. R. Isidoro, Shadow mapping: Gpu-based tips and techniques, 2006.
- 538 [32] A. M. Elmalky, M. T. Araji, Computational procedure of solar irradiation: A new approach for high performance façades with experimental
539 validation, *Energy and Buildings* 298 (2023) 113491.
- 540 [33] B. R. Vatti, A generic solution to polygon clipping, *Communications of the ACM* 35 (7) (1992) 56–63.
- 541 [34] A. Arias-Rosales, P. R. LeDuc, Shadow modeling in urban environments for solar harvesting devices with freely defined positions and
542 orientations, *Renewable and Sustainable Energy Reviews* 164 (2022) 112522. doi:[10.1016/j.rser.2022.112522](https://doi.org/10.1016/j.rser.2022.112522).
- 543 [35] W. Liao, Y. Heo, S. Xu, Simplified vector-based model tailored for urban-scale prediction of solar irradiance, *Solar Energy* 183 (2019)
544 566–586.
- 545 [36] F. Biljecki, H. Ledoux, J. Stoter, Does a finer level of detail of a 3d city model bring an improvement for estimating shadows?, *Advances in*
546 *3D geoinformation* (2017) 31–47.
- 547 [37] E. Garreau, T. Berthou, B. Duplessis, V. Partenay, D. Marchio, Solar shading and multi-zone thermal simulation: Parsimonious modelling at
548 urban scale, *Energy and Buildings* 249 (2021) 111176. doi:[10.1016/j.enbuild.2021.111176](https://doi.org/10.1016/j.enbuild.2021.111176).
- 549 [38] X. Faure, T. Johansson, O. Pasichnyi, The impact of detail, shadowing and thermal zoning levels on urban building energy modelling (UBEM)
550 on a district scale, *Energies* 15 (4) (2022) 1525. doi:[10.3390/en15041525](https://doi.org/10.3390/en15041525).
- 551 [39] Z. Liu, X. Liu, H. Zhang, D. Yan, Integrated physical approach to assessing urban-scale building photovoltaic potential at high spatiotemporal
552 resolution, *Journal of Cleaner Production* 388 (2023) 135979. doi:[10.1016/j.jclepro.2023.135979](https://doi.org/10.1016/j.jclepro.2023.135979).
- 553 [40] Z. Zheng, J. Chen, X. Luo, Parallel computational building-chain model for rapid urban-scale energy simulation, *Energy and Buildings* 201
554 (2019) 37–52. doi:[10.1016/j.enbuild.2019.07.034](https://doi.org/10.1016/j.enbuild.2019.07.034).

- 555 [41] I. Maestre, L. Pérez-Lombard, J. Foncubierta, P. Cubillas, Improving direct solar shading calculations within building energy simulation tools,
556 Journal of building performance simulation 6 (6) (2013) 437–448.
- 557 [42] X. Wang, X. Zhang, S. Zhu, J. Ren, F. Causone, Y. Ye, X. Jin, X. Zhou, X. Shi, A novel and efficient method for calculating beam shadows on
558 exterior surfaces of buildings in dense urban contexts, Building and Environment 229 (2023) 109937. doi:10.1016/j.buildenv.2022.
559 109937.
- 560 [43] D. Yan, J. Xia, W. Tang, F. Song, X. Zhang, Y. Jiang, DeST — an integrated building simulation toolkit part i: Fundamentals, Building
561 Simulation 1 (2) (2008) 95–110. doi:10.1007/s12273-008-8118-8.
- 562 [44] N. Mohajeri, G. Upadhyay, A. Gudmundsson, D. Assouline, J. Kämpf, J.-L. Scartezzini, Effects of urban compactness on solar energy
563 potential, Renewable Energy 93 (2016) 469–482.
- 564 [45] F. Biljecki, Y. S. Chow, Global building morphology indicators, Computers, Environment and Urban Systems 95 (2022) 101809.
- 565 [46] F. Bu, X. Kang, D. Yan, R. Wu, H. Sun, J. An, X. Wang, Acceleration of state-space method based on parallelization for enhancing building
566 thermal process simulation efficiency, Energy and Buildings (2023) 113600.
- 567 [47] J. Robledo, J. Leloux, E. Lorenzo, C. A. Gueymard, From video games to solar energy: 3d shading simulation for pv using gpu, Solar Energy
568 193 (2019) 962–980.
- 569 [48] Y. Huang, Z. Chen, B. Wu, L. Chen, W. Mao, F. Zhao, J. Wu, J. Wu, B. Yu, Estimating roof solar energy potential in the downtown area using
570 a gpu-accelerated solar radiation model and airborne lidar data, Remote Sensing 7 (12) (2015) 17212–17233.